Electrodynamics of the vanadium oxides VO_2 and V_2O_3

M. M. Qazilbash,[1,*] A. A. Schafgans,[1] K. S. Burch,[1,†] S. J. Yun,[2] B. G. Chae,[2] B. J. Kim,[2] H. T. Kim,[2] and D. N. Basov[1]
[1]*Physics Department, University of California–San Diego, La Jolla, California 92093, USA*
[2]*IT Convergence and Components Lab, ETRI, Daejeon 305-350, Korea*

(Received 19 September 2007; revised manuscript received 7 January 2008; published 17 March 2008)

The optical and infrared properties of films of vanadium dioxide (VO_2) and vanadium sesquioxide (V_2O_3) have been investigated via ellipsometry and near-normal incidence reflectance measurements from far infrared to ultraviolet frequencies. Significant changes occur in the optical conductivity of both VO_2 and V_2O_3 across the metal-insulator transitions at least up to (and possibly beyond) 6 eV. We argue that such changes in optical conductivity and electronic spectral weight over a broad frequency range are evidence of the important role of electronic correlations to the metal-insulator transitions in both of these vanadium oxides. We observe a sharp optical transition with possible final state (exciton) effects in the insulating phase of VO_2. This sharp optical transition occurs between narrow a_{1g} bands that arise from the quasi-one-dimensional chains of vanadium dimers. Electronic correlations in the metallic phases of both VO_2 and V_2O_3 lead to reduction of the kinetic energy of the charge carriers compared to band theory values, with paramagnetic metallic V_2O_3 showing evidence of stronger correlations compared to rutile metallic VO_2.

DOI: 10.1103/PhysRevB.77.115121 PACS number(s): 71.30.+h, 71.27.+a, 78.20.−e, 78.30.−j

I. INTRODUCTION

Vanadium dioxide (VO_2) and vanadium sesquioxide (V_2O_3) have been the subjects of intensive experimental and theoretical studies for the past several decades. These systems are considered classical prototypes of materials exhibiting metal-insulator transitions.[1,2] An interesting and intriguing aspect is that the electronic metal-insulator transitions in VO_2 and V_2O_3 are accompanied by changes in the lattice structure. While there has been progress toward understanding the roles played by electron-electron interactions and the lattice distortion in the metal-insulator transitions, there is no consensus on the mechanism of the metal-insulator transitions, at least in the case of VO_2. An important difference between the two oxides is that V_2O_3 is antiferromagnetically ordered in the insulating phase whereas the most stable insulating phase (M_1) of VO_2 does not exhibit magnetic ordering. In M_1 VO_2, the Peierls distortion leads to dimerization (pairing or charge ordering) of vanadium ions[3] thereby preventing magnetic ordering in an otherwise correlated insulator.[1,4] Another difference between these two oxides is that the nominal valence of vanadium ions in VO_2 is +4 whereas in V_2O_3 it is +3.

VO_2 undergoes a metal-insulator transition (MIT) at $T \approx 340$ K from a low temperature insulating phase to a high temperature rutile metallic phase. The resistivity decreases by four orders of magnitude across the MIT accompanied by a structural transition from the monoclinic unit cell in the insulator (M_1) to a tetragonal unit cell in the rutile metal (R). In VO_2, the vanadium ions are in the +4 valence state, and therefore a single electron resides in the d orbitals, a scenario supported by theoretical calculations and by recent experiments.[5–9] There has been much controversy on the driving mechanism of the MIT in VO_2, and over the relative importance of the Peierls scenario within the single particle picture and electronic correlations representing Mott physics.[5–9,11–21] We have recently demonstrated divergent effective quasiparticle mass in VO_2 as evidence that the MIT is a Mott transition.[22–24] There is, however, a structural component to the phase transition in the form of a Peierls instability (charge density wave) in the monoclinic insulating (M_1) phase of VO_2 which leads to unit cell doubling and the formation of vanadium dimers (pairs) along the c axis (in the rutile basis). The presence of such vanadium chains imparts a quasi-one-dimensional character to what is essentially a three-dimensional system. The competing effect of the Peierls instability prevents long-range magnetic ordering in the correlated M_1 phase of VO_2. Therefore, the M_1 phase of VO_2 should be classified as a Mott insulator that is charge ordered and not magnetically ordered.[22]

V_2O_3 undergoes a first-order metal-insulator transition at $T \approx 150$ K from a low temperature antiferromagnetic insulating (AFI) phase to a high temperature paramagnetic metallic (PMM) phase. The crystal structure also deforms from monoclinic in the insulating phase to rhombohedral symmetry in the metallic phase. The V-V distance along the c axis (in hexagonal basis) is larger in the monoclinic insulating phase compared to the rhombohedral metal.[25] While there is debate on the significance of cation-cation covalent bonding along the c axis to the physics of V_2O_3,[26–31] the change in crystal structure of V_2O_3 is not associated with Peierls instability and unit-cell doubling, and magnetic ordering is preserved in the insulating phase. From charge balancing in the chemical formula of V_2O_3, the vanadium ions are in the +3 valence state and two electrons are present in the d orbitals of vanadium. Despite extensive experimental and theoretical effort, there is no consensus on precisely how the two electrons are distributed within the t_{2g} manifold of the d levels.[26–35] There is, however, an agreement that the single-band Hubbard model is inadequate to describe the MIT in V_2O_3 given the complex multiorbital character of this material. The experimental results reported here provide further constraints on the intrinsic electronic structure of the PMM and AFI phases of V_2O_3.

Given that both of these oxides of vanadium exhibit metal-insulator transitions that are accompanied by changes in lattice structure, it is important to understand, on the same footing, their optical properties across the phase transition. A

comprehensive study of the optical properties of VO_2 and V_2O_3 will help us gain insight into how charge ordering in insulating VO_2 and magnetic ordering in insulating V_2O_3 influence the electrodynamics of their respective insulating phases and the neighboring metallic phases. There have been several previous studies that have addressed the optical properties of VO_2 and/or V_2O_3.[36–44] However, none of these studies have reported optical constants of both VO_2 and V_2O_3 over the wide frequency [far infrared to ultraviolet (6 eV)] and temperature ranges that we have been able to investigate in this work.

We find that VO_2 and V_2O_3 are correlated materials in which the important energy scale is the Hubbard intra-atomic Coulomb repulsion energy U leading to changes in optical conductivity and spectral weight at least up to 6 eV. We find that M_1 VO_2, a Mott insulator that is charge ordered, exhibits a sharp, distinct feature in the optical conductivity that likely results from the quasi-one-dimensional character of the density of states related to the one-dimensional chains formed by vanadium pairs. We discuss the possibility that this feature in the optical conductivity of VO_2 also has an excitonic origin due to final state effects. Such a distinct feature is absent in the optical conductivity of the Mott insulator V_2O_3, which is magnetically ordered and lacks the quasi-one-dimensional character associated with charge ordering. Charge ordering in insulating VO_2 may partially circumvent the effects of the intra-atomic Coulomb repulsion or Hubbard U.[45] Nevertheless, the intra-atomic Coulomb repulsion is necessary for opening the energy gap in M_1 VO_2 as well as in AFI V_2O_3. Moreover, electronic correlations dominate charge dynamics in the metallic phases of both VO_2 and V_2O_3, with PMM V_2O_3 more strongly correlated compared to rutile VO_2.

II. EXPERIMENTAL METHODS

Previous optical and infrared studies on V_2O_3 crystals addressed the issue of changes in spectral weight across the MIT in the energy range up to $\approx$1.5 eV.[39–42] The availability of high quality V_2O_3 and VO_2 films and recent advances in broadband ellipsometry at cryogenic and elevated temperatures enable accurate determination of optical constants and changes in spectral weight with temperature over a wide energy (frequency) range.[46] This is because ellipsometry is a self-referencing measurement and the complex ellipsometric constants [real part $\Psi(\omega)$ and imaginary part $\Delta(\omega)$] can be obtained at each incident frequency thereby precluding the need for Kramers-Kronig transformations.[47] The MIT is literally destructive for pure VO_2 and V_2O_3 crystals, which could make accurate measurements in both metallic and insulating states on the same sample very challenging. The VO_2 and V_2O_3 films, on the other hand, do not show signs of deterioration even after going through several cycles across the MIT.[48]

VO_2 films about 100 nm thick were grown on $(\bar{1}012)$ oriented sapphire (Al_2O_3) substrates by the sol-gel method and the details of growth and characterization are given elsewhere.[49] Films of V_2O_3 are 75 nm thick and are grown on $(10\bar{1}0)$ oriented sapphire substrates. The V_2O_3 films are obtained by annealing VO_2 films at 600 °C for 30 min in a vacuum chamber where the pressure is maintained in the order of 10^{-6} torr.[50] The VO_2 films are grown by the sol-gel method on $(10\bar{1}0)$ oriented sapphire substrates[49] and were used as the starting material in order to obtain crystalline V_2O_3 films. The films were confirmed by x-ray diffraction to be single phase V_2O_3. The resistivity of the V_2O_3 films shows a decrease of more than four orders of magnitude in the metallic phase compared to the insulating phase with T_c=150 K at the midpoint of the MIT (in the heating cycle) in good agreement with previous reports.[51] Although the VO_2 and V_2O_3 films are polycrystalline, the MIT characteristics closely resemble properties of bulk samples.[49–51]

The optical constants of the VO_2 films were obtained from ellipsometric data (50 meV–6 eV) and near-normal incidence reflectance data (5–80 meV) in the insulating and metallic states. The optical constants of V_2O_3 films were obtained from a combination of ellipsometric measurements and near-normal incidence reflectance, with ellipsometric data covering most of the frequency range. Ellipsometric data were obtained from 0.6–6 eV for T=100–400 K, and from 50 meV–0.7 eV for T=300–400 K. Reflectance data were obtained from 50 meV to 0.7 eV from T=100–300 K, and from 6–80 meV in the temperature range T=100–400 K. Unlike previous optical studies on single crystals, the VO_2 and V_2O_3 films were not subject to surface treatment (polishing, etc.) which could affect the spectra in the visible-ultraviolet spectral range. Therefore the optical constants are those of the pristine as-grown films.

The real and imaginary parts of the ellipsometric constants of the VO_2 and V_2O_3 films on sapphire substrates were measured for two angles of incidence (60° and 75°). The complex optical constants (and subsequently the complex conductivities) of VO_2 and V_2O_3 were obtained via the analysis of a two-layer model of a film layer on an infinitely thick substrate. The latter aspect of the model is valid for a substrate with rough back surface, which prevents coherent back reflections.[47,52] Details of the ellipsometric measurements at cryogenic temperatures on V_2O_3 are given in the Appendix. The electromagnetic response of the VO_2 and V_2O_3 films is modeled using Drude, Lorentzian, and Tauc-Lorentzian oscillators. The complex optical constants of the bare sapphire substrate have been obtained via ellipsometric, near-normal incidence reflectance, and normal-incidence transmission measurements and were incorporated into the model.[53] The absolute near-normal incidence reflectance measurements on the VO_2 and V_2O_3 films were performed using *in situ* evaporated gold film as a reference. The reflectance data were analyzed together with ellipsometric data using the same two-layer model as described previously. The contributions of VO_2 and V_2O_3 phonons to the optical constants in the spectral range $\approx$20–100 meV were modeled by Lorentzian oscillators. Subsequently, these phonon contributions were subtracted and only the electronic contribution to the optical constants of VO_2 and V_2O_3 is presented and analyzed in this work. We note that the spectral weight of the VO_2 and V_2O_3 phonons is negligibly small compared to the electronic spectral weight, and therefore we will not be concerned with the phonon spectral weight in this work.[54]

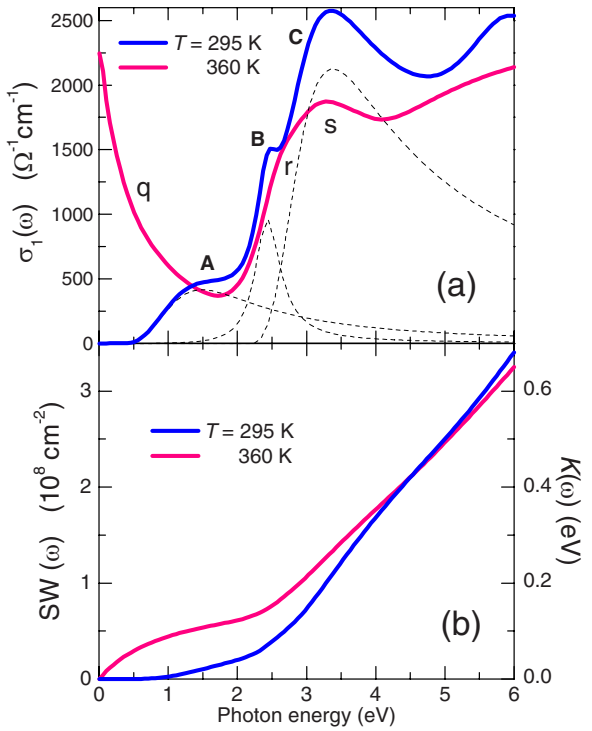

FIG. 1. (Color online) (a) Real part of the conductivity $\sigma_1(\omega)$ of VO_2 plotted as a function of photon energy for the M_1 insulating phase (T=295 K) and the rutile metallic phase (T=360 K). The labels in uppercase and lowercase letters refer to features in $\sigma_1(\omega)$ in the insulating phase and metallic phase, respectively. The dashed curves represent the optical transitions that contribute to features "A," "B," and "C" in $\sigma_1(\omega)$ in the insulating phase (see the text for details). (b) The spectral weight $SW(\omega)$ is plotted as a function of photon energy for the insulating and rutile metallic phases of VO_2. The spectral weight is also plotted in units of energy $K(\omega)$ defined in Eq. (2).

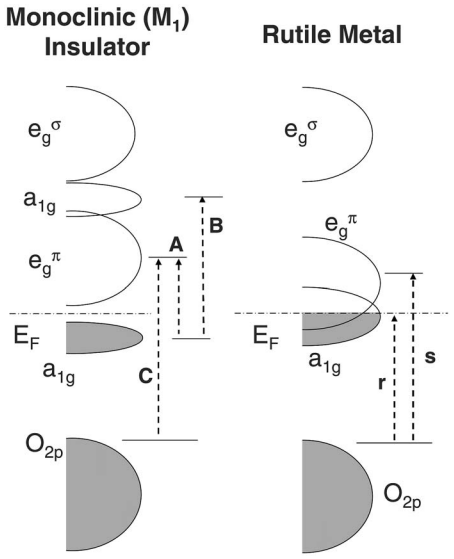

FIG. 2. Energy level diagrams for the monoclinic insulating (M_1) phase and rutile metallic (R) phase of VO_2 showing the relevant vanadium and oxygen energy levels and optical transition energies. E_F denotes the Fermi level. The energy level diagram in the M_1 phase is based on the results of this work and Refs. 9 and 10 and includes the effect of U on the t_{2g} bands. The energy level diagram of the rutile metal is based on this work as well as band theory calculations that give the relative separation between the t_{2g} (a_{1g},e_g^π), e_g^σ, and O_{2p} bands.[5,6] However, the effect of U on the t_{2g} bands in the rutile metal is not explicitly included in band theory calculations and may lead to a Hubbard splitting of the a_{1g} band.[7] In this case, the feature "r" in Fig. 1(a) may alternatively arise from an optical transition between the lower and upper Hubbard bands.

III. RESULTS ON VO_2

In Fig. 1(a), we plot the real part of the optical conductivity $\sigma_1(\omega)$ of the M_1 insulating phase (T=295 K) and rutile metallic phase (T=360 K) of a VO_2 film. The features in $\sigma_1(\omega)$ of the insulating and metallic phases will be explained within the model of energy levels shown in Fig. 2. According to band theory calculations and photoemission data,[5,6,9,38,55] the O_{2p} bands lie between 2 and 8 eV below the Fermi energy in both the insulating and metallic phases. Also, within band theory calculations, the crystal field splits the degenerate d orbitals into t_{2g} bands and e_g^σ bands. The former are lower in energy and contain the single d electron. The t_{2g} bands are further split into an a_{1g} band and e_g^π bands, with the latter centered at higher energy compared to the former. We follow Ref. 7 in using the terminology a_{1g} and e_g^π. The a_{1g} band further splits into what we call the lower a_{1g} band and the upper a_{1g} band in the M_1 insulator. In the Mott picture, these can be considered as lower and upper Hubbard bands while in the Peierls model, these are the bonding and antibonding bands, respectively.[3,4] The energy gap of 0.6 eV in the monoclinic (M_1) insulating phase is between the filled a_{1g} band and the empty e_g^π band. Peierls physics alone cannot explain this large energy gap as pointed out by Mott.[4] Various LDA calculations repeatedly fail to confirm this large energy gap.[5,6] The failure of LDA to account for a gap in insulating VO_2 has been attributed to the shortcomings of LDA in predicting band gaps correctly.[5] However, an energy gap of correct magnitude does appear once correlation effects (Hubbard U) are taken into account.[7,45] In the rutile metal, the energy gap collapses and the Fermi level crosses partially filled a_{1g} and e_g^π bands (see Fig. 2).[3–7]

We attempt to explain the various features in the optical spectra of VO_2 (and subsequently of V_2O_3) by comparing our data to previous theoretical and experimental reports. Peaks at finite energies in the optical conductivity occur when there are direct optical transitions between filled and empty bands in a solid. More precisely, the interband optical transitions are governed by the electric dipole transition matrix elements and peaks in the joint density of (filled and empty) states. The hump feature in Fig. 1(a) labeled "A" at 1.4 eV is due to optical transitions from the filled lower a_{1g} band to the empty e_g^π bands across an optical gap of $\approx$0.5 eV. It is appropriate to attribute peak "B" at 2.5 eV to transitions from the narrow lower filled a_{1g} band to the narrow upper empty a_{1g} band. Peak "C" at 3.2 eV is due to transitions from the filled O_{2p} bands and empty e_g^π bands. We do not observe any obvious signs of optical transitions from the O_{2p} bands to the empty a_{1g} band which are expected at $\approx$4.7 eV, and this is likely due to diminished overlap be-

tween the a_{1g} and O_{2p} orbitals in the insulating state of VO_2.

A broad Drude-type feature is observed in the optical conductivity of the rutile metallic phase (labeled "*q*"). The spectral weight in the Drude-type peak is borrowed from the optical transitions at frequencies higher than 1.3 eV, the energy at which the two solid curves in Fig. 1(a) cross. We see a weak shoulder "*r*" at 2.6 eV and a peak "*s*" at 3.1 eV which we attribute to optical transitions from the O_{2p} bands to partially filled a_{1g} and e_g^{π} bands, respectively. Compared to the monoclinic insulator, the optical transitions from O_{2p} to the a_{1g} band become apparent in the rutile metal possibly because of increased overlap between the O_{2p} and a_{1g} orbitals. An alternative explanation of the shoulder feature labeled *r* is that it arises from optical transitions between remnants of the lower Hubbard band and upper Hubbard band in the rutile metal. We note that while the lower Hubbard band is seen by photoemission, a feature due to the upper Hubbard band is absent in the x-ray absorption data.[9]

At this point we remark that compared to the broader peaks *A* and *C* in $\sigma_1(\omega)$ in the insulating phase, peak *B* is unusually narrow. This is more so in the case of VO_2 film grown on $(10\bar{1}0)$ sapphire whose optical conductivity we published in a previous work.[56] In fact, peak *B* is described by a nearly Lorentzian line shape with half-width of 0.5 eV, which is much narrower compared to the corresponding width parameters of the Tauc-Lorentzian oscillators[57] used to describe peaks *A* ($\approx$1.6 eV) and *C* ($\approx$1.4 eV). The quasi-one-dimensional nature of the V-V chains leads to narrow upper and lower a_{1g} bands and a sharp optical transition between these bands. In addition, it is possible that peak *B* is excitonic in nature,[37] such that the optical transition between the filled and empty a_{1g} bands is redshifted by the electron-hole binding energy due to Coulomb attraction. Such an electron-hole pair is described as a charge-transfer exciton[58] whose spatial extent lies somewhere between the Mott-Wannier exciton that is delocalized over several unit cells and the Frenkel exciton that is confined to an atom or molecule. The charge-transfer exciton is likely localized on the vanadium dimer whose V-V separation is 2.65 Å, and thus is more closely related to the Frenkel exciton. The charge-transfer exciton is not present in the rutile metallic phase and this could be due to one or more of the following reasons: merger of the lower and upper a_{1g} levels, absence of long-range charge ordering, and screening due to mobile charge carriers.

We make use of the model that is applicable to Mott-Wannier excitons to estimate the binding energy (E_b) of the charge-transfer exciton. It is not obvious if this model is applicable to the charge-transfer exciton in VO_2 because of the exciton's localized character. However, the model appears to provide a reasonable description of charge-transfer excitons in alkali halides and pentacene, for example.[59] The binding energy is given by $E_b = \frac{e^2}{\epsilon r_{eh}}$ where *e* is the electron charge, ϵ is the static dielectric constant of VO_2 ($\epsilon \approx 20$), and r_{eh} is the separation between the electron-hole pair in the exciton and is taken to be 2.65 Å, which is the V-V distance in the dimer. We hence obtain $E_b \approx 0.27$ eV. Therefore, we estimate the actual energy separation between the lower and upper a_{1g} levels to be 2.8 eV. The photoemission and polarized x-ray absorption data suggest that the separation between the a_{1g} levels is indeed 2.5–2.8 eV.[9] It appears that the higher estimate is closer to the picture we present here. The half-width of the a_{1g} bands in Ref. 9 is $\approx$1 eV. Interband transitions between the lower and upper a_{1g} energy levels would then be expected to be described by a Lorentzian oscillator with a half-width of at least 1 eV. However, peak *B* is described by a Lorentzian oscillator with a half-width of $\approx$0.5 eV, which lends support to the hypothesis that it is excitonic in nature. We note that the assignment of the interband transitions *A*, *C*, *r*, and *s* are also consistent with the photoemission and x-ray absorption data.[9]

Calculations for the separation of a_{1g} levels in the V-V dimer start with considering a "hydrogen molecule" model of the dimer.[45] With the intra-atomic Coulomb repulsion *U* set to 4.0 eV and the LDA hopping (*t*) to 0.7 eV, the a_{1g}-a_{1g} separation is given by $\Delta_{a_{1g}} = -2t + 4t\sqrt{1+(U/4t)^2} = 3.48$ eV. This value of *U* is required to open an energy gap of the correct magnitude in insulating VO_2. The calculated value for $\Delta_{a_{1g}}$ is expected to be reduced to 3 eV due to effects not accounted for by the above simple model and discussed in Ref. 45. The actual position of peak *B* at 2.5 eV is less than the theory value of the a_{1g}-a_{1g} energy separation. This further supports the notion of its excitonic origin due to final state effects of electron-hole Coulomb attraction that are not accounted for in Ref. 45.

We now discuss the spectral weight changes across the MIT in VO_2. The oscillator strength sum rule (or *f*-sum rule) is a fundamental statement on the conservation of charge in a material. The most generic form employs the integral of the real part of the optical conductivity $\sigma_1(\omega)$ over all frequencies as follows:

$$\int_0^{\infty} \sigma_1(\omega) d\omega = \frac{\pi n e^2}{2m_e}. \tag{1}$$

Here, *n* is the density of electrons and m_e is the free electron mass. In reality, however, we study spectral weight changes up to a finite frequency, which in our experiments is 6 eV, and we can comment upon whether or not the *f*-sum rule is satisfied in this frequency window. We plot the spectral weight $SW(\omega) = \int_0^{\omega} \sigma_1(\omega') d\omega'$ in Fig. 1(b) for VO_2. The right-hand vertical axis in Fig. 1(b) shows the spectral weight as an energy $K(\omega)$ in units of eV, which can readily be compared to band theory values. Following Millis *et al.*, the energy $K(\omega)$ is given by[60]

$$K(\omega) = \frac{\hbar a}{e^2} \int_0^{\omega} \frac{2\hbar}{\pi} \sigma_1(\omega') d\omega'. \tag{2}$$

Here *a* is the lattice constant which is taken as $\approx$3 Å, the average V-V distance in both VO_2 and V_2O_3. Also note that $\hbar/e^2 = 4.1$ kΩ.

Figures 1(a) and 1(b) show that the spectral weight in the broad Drude-type part of the conductivity in the rutile metal is obtained from the loss of spectral weight of the peaks *A*, *B*, and *C* in the insulator. In the rutile metal, the e_g^{π} bands and the a_{1g} band are both partially occupied (see Fig. 2). Therefore, the optical transition (peak *s*) from the O_{2p} to the e_g^{π}

band has reduced spectral weight in the rutile metal compared peak C in the insulator. The changes in spectral weight across the MIT extend up to and beyond 6 eV. We note that interband transitions between the filled O_{2p} and empty e_g^σ levels may occur above 4 eV but are not expected to change across the MIT. Interband transitions between filled t_{2g} and empty e_g^σ are expected at $\approx$6 eV ($U \approx 4$ eV in addition to 2 eV crystal field splitting)[61] and are likely to be modified by the MIT because of the rearrangement of t_{2g} bands. Thus the changes in optical conductivity and spectral weight that occur above 4 eV across the MIT can be attributed to changes in optical transition probabilities from filled t_{2g} states to empty e_g^σ states. The rather large energy scale over which changes in $SW(\omega)$ are seen across the metal-insulator transition ought to be taken as direct evidence for the predominance of correlation effects, and hence an indication of a Mott transition. Similar large energy scales are involved in spectral weight changes in doped Mott insulators, for example, in the cuprates.[2,63] We find that the Hubbard parameter U determines, to a large extent, the energy scale over which $SW(\omega)$ changes take place across the MIT in VO_2. The Peierls instability within the single-particle scenario alone would result in rearrangement of the t_{2g} bands within $\approx$1 eV of the Fermi energy. Then the scale over which changes in spectral weight occur would be $\approx$3 eV and determined by the interband transitions between O_{2p} and t_{2g} bands and between t_{2g} and e_g^σ bands (without Hubbard U). Thus changes in $\sigma_1(\omega)$ and $SW(\omega)$ that occur well beyond 3 eV provide direct evidence of the importance of correlation effects (Hubbard U) to the MIT in VO_2.

The energy $K(\omega)$ associated with the intraband conductivity (the broad Drude-type feature) in VO_2 is $\approx$0.12 eV and can be considered as the kinetic energy of delocalized charge carriers.[62] The kinetic energy is determined by setting the intraband cutoff energy at 1.7 eV where the minimum in $\sigma_1(\omega)$ occurs. The kinetic energy of the delocalized carriers is nearly fifty percent of the band theory value.[5,56,64] Correlations among electrons are expected to reduce their kinetic energy compared to that predicted by band theory.[60,62] On the other hand, in the presence of electron-phonon interactions, the ground state wave function and hence the kinetic energy of the electrons is essentially that given by band theory.[62] An exception to this occurs in the presence of very strong electron-phonon coupling, which can cause a significant reduction in the electronic kinetic energy and likely leads to a polaronic insulating state. However, this scenario is not realized in the rutile phase of VO_2, which is clearly metallic. Therefore, the reduction in kinetic energy of the electrons clearly points to the dominance of correlation effects to the charge dynamics in rutile metallic VO_2. In addition, it was shown in Ref. 56 that the form of the frequency-dependent scattering rate cannot be explained by electron-phonon scattering alone, and that electronic correlations must also influence the charge dynamics. More recently, divergent optical mass was inferred in the metallic nanoscale islands that form in the insulating host at the onset of the MIT in VO_2.[22] This observation is strong evidence for the importance of Mott physics to the insulating and metallic phases in the vicinity of the MIT in VO_2.

IV. RESULTS ON V_2O_3

We now turn to the real part of optical conductivity $\sigma_1(\omega)$ of V_2O_3 plotted in Fig. 3(a). As in VO_2, there is rearrangement of $\sigma_1(\omega)$ and $SW(\omega)$ across the MIT. In the insulating phase of V_2O_3 at $T=100$ K, there is an optical gap of $\approx$0.5 eV followed by interband transitions labeled D to H. Because there are two valence d electrons per vanadium ion in V_2O_3, V-V intersite transitions are expected at multiple energies and hence multiple peaks occur in the conductivity data up to 3.5 eV.[61] The energy band diagram for V_2O_3 in Fig. 4 gives the relative energy separation between the O_{2p} and vanadium t_{2g} bands and is a rough guide for the interband transitions and the changes that take place across the MIT. The photoemission data and band structure calculations show that the O_{2p} bands lie between 3.5 and 8.5 eV below the Fermi energy.[38,65] Then the rise in optical conductivity starting from $\approx$4 eV is due to interband transitions from the O_{2p} to the empty t_{2g} orbitals on the vanadium sites. Specifically, the distinct shoulderlike structure H in the AFI spectrum can be attributed to such interband transitions. The crystal field splits the vanadium d bands into e_g^σ bands that are centered $\approx$3 eV above the t_{2g} bands.[27,65] The lower symmetry of the rhombohedral lattice lifts the degeneracy of the t_{2g} bands, which evolve into nondegenerate a_{1g} and doubly degenerate e_g^π bands.[27]

We focus our attention on the optical transitions within the vanadium t_{2g} manifold, which are better described by considering intersite transitions in real space rather than by appealing to energy bands. This is because in V_2O_3, two d electrons are believed to be distributed in the e_g^π and a_{1g} bands in a nontrivial manner.[26–35] Lee *et al.* have discussed, on general physical grounds, the optical excitations in transition metal oxides with multiorbital character.[61] However, their classification scheme does not take into account explicitly the lifting of degeneracy of the t_{2g} orbitals due to crystal field splitting, which may be relevant for identification of the intersite transitions in V_2O_3. Therefore, assignment of the various interband transitions in both the AFI and PMM phases is difficult without a quantitative model specific to V_2O_3. Nevertheless, relevant physical parameters for V_2O_3 can be estimated from our data based on the classification scheme of Lee *et al.* We note that for two valence electrons in the t_{2g} manifold, the minimum and maximum allowed optical transition energies are given by $U-3J_H$ and $U+2J_H$, respectively, while assuming the crystal field splitting is less than the other relevant parameters in the system (U, J_H, and bandwidth). Here, U is the intra-atomic Coulomb repulsion and J_H is the Hund's rule exchange energy. Then the lowest energy peak D at 1.2 eV in the AFI spectrum is the optical transition given by $U-3J_H$ and the energy peak G at 3.6 eV is given by $U+2J_H$. This gives $U \approx 2.6$ eV and $J_H \approx 0.5$ eV. These numbers are toward the lower end of the spectrum of values that appear in the extensive literature on V_2O_3 (for example, see Ref. 30). It is likely that we have estimated the screened value of U while the unscreened value could be 4–5 eV.[27] We note that in the antiferromagnetic insulator, each vanadium ion has one nearest neighbor with spin

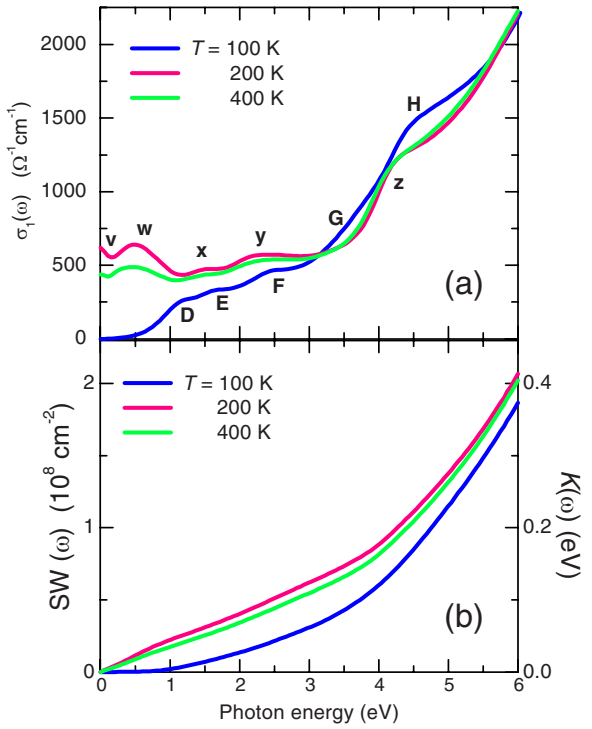

FIG. 3. (Color online) Real part of the conductivity $\sigma_1(\omega)$ of V_2O_3 plotted as a function of photon energy for the insulating phase (T=100 K) and for two temperatures in the metallic phase (T=200 and 400 K). The labels in uppercase and lowercase letters refer to features in $\sigma_1(\omega)$ in the insulating phase and metallic phase, respectively. (b) The spectral weight $SW(\omega)$ is plotted as a function of photon energy for selected temperatures. The spectral weight is also plotted in units of energy $K(\omega)$ defined in Eq. (2).

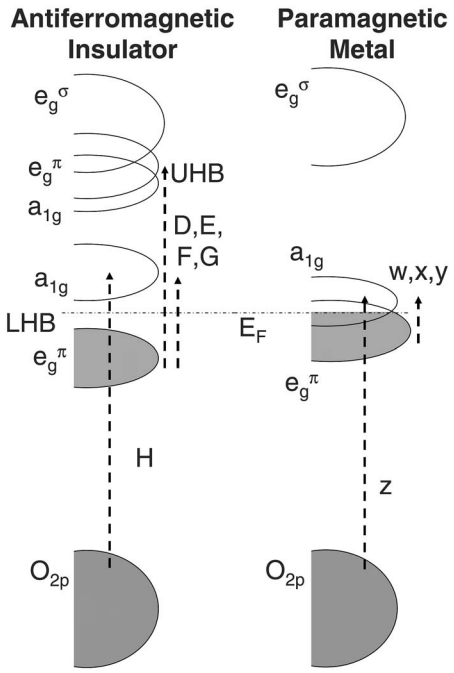

FIG. 4. Energy level diagrams for the antiferromagnetic insulating (AFI) phase and paramagnetic metallic (PMM) phase of V_2O_3 showing the relevant vanadium and oxygen energy levels and optical transitions. LHB and UHB refer to the lower Hubbard bands, and upper Hubbard bands, respectively. E_F denotes the Fermi level. The energy level diagram for the AFI is based on the LDA+U calculations.[27] For the PMM energy levels we rely on LDA calculations,[65] but we note that the persistence of interband transitions between the vanadium t_{2g} orbitals in $\sigma_1(\omega)$ in the PMM suggests the importance of the Hubbard U, which is not accounted for within LDA. Our work and Ref. 38 confirm the relative separation of the O_{2p} and vanadium t_{2g} (a_{1g} and e_g^{π}) bands.

aligned in the same direction and two nearest neighbors with spins antialigned. Also, because there are no definitive reports on orbital ordering in AFI, all allowed optical transitions should appear in the spectra of the AFI.[61] We also note here that for reasons given earlier for VO_2, the transitions from O_{2p} and t_{2g} bands to the e_g^{σ} bands lie close to and beyond the energy cutoff of 6 eV in our experiment.[61] The spectral features due to intersite transitions between the t_{2g} orbitals of the vanadium ions in V_2O_3 closely resemble those seen in the Mott insulator YVO_3 in which the vanadium ions also have two d electrons in the t_{2g} orbitals.[46] In YVO_3, the spectral features between 1 and 4 eV were also assigned to intersite transitions between the t_{2g} orbitals.

From Figs. 3(a) and 3(b) one can see that there is significant rearrangement of the conductivity spectra across the MIT. A weak Drude peak labeled v and a finite energy mode at 0.5 eV labeled w emerge in the metallic phase together with spectral weight enhancement of other interband transitions below 3 eV. In the PMM state, the spectral weight due to the shoulderlike features G and H decreases. The peaks E, F, and H in the AFI spectrum shift downwards by 0.2–0.3 eV and are labeled as x, y, and z, respectively, in the spectra for PMM. This downward shift could be due to the reduction of crystal field splitting between the a_{1g} and e_g^{π} levels. The reduced spectral weight of the z feature in PMM compared to the H feature in AFI is due to the partial occupation of the a_{1g} band in the PMM phase. The decrease in the spectral weight of the $U+2J_H$ transition (feature G) is due to the absence of antiferromagnetic ordering in PMM. Moreover, it appears that ferromagnetic correlations (not ordering) persist in the PMM because of the increase in the optical conductivity (and spectral weight) between 1 and 3 eV compared to the AFI. This is because for ferromagnetic correlations, the optical transitions between U and $U-3J_H$ will be favored compared to those between U and $U+2J_H$.[32,66,67] Moreover, orbital switching effects could also contribute to the increased optical conductivity between 1 and 3 eV in the PMM.[67]

The Drude peak in the PMM arises from intraband dynamics of coherent quasiparticles of a_{1g} character. This is firmly supported by DMFT calculations in the PMM state.[68] Since the spectral weight of the Drude peak is low, we surmise that the density of coherent quasiparticles is rather low and/or their mass is quite high. Nevertheless the presence of the Drude peak in metallic V_2O_3 with dc conductivity below that of the apparent Ioffe-Regel-Mott limit (4000 Ω^{-1} cm^{-1}) of metallic transport is remarkable.[56] Next, it appears that the majority of the charge carriers are completely incoherent and reside in the e_g^{π} bands.[68] These likely contribute a broad background to the conductivity and do not give rise to any

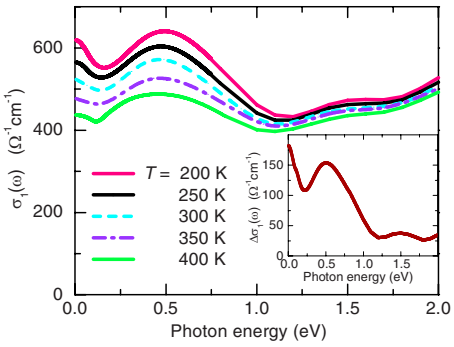

FIG. 5. (Color online) Temperature dependence of the real part of the optical conductivity $\sigma_1(\omega)$ of the metallic phase (PMM) of V_2O_3 plotted as a function of the incident photon energy up to 2 eV. The inset shows the difference in the optical conductivities of PMM between the lowest and highest temperatures $\Delta\sigma_1(\omega) = \sigma_1(\omega, T=200\ \mathrm{K}) - \sigma_1(\omega, T=400\ \mathrm{K})$.

particular feature in the PMM optical conductivity. The charge dynamics in the dc limit is then dominated by the coherent a_{1g} quasiparticles. The peak w can be assigned to intersite transitions between incoherent e_g^π carriers and partially occupied coherent a_{1g} orbitals.

In Fig. 3(b), we see that there is more spectral weight in the metallic phase ($T=200$ K) at low energies compared to the insulating phase ($T=100$ K) and that this extra spectral weight is never fully recovered in the insulating phase up to 6 eV. The additional spectral weight in PMM up to 3 eV is partly borrowed from optical transitions G and H in AFI. The rest is probably borrowed from higher-lying optical transitions (>6 eV) in the AFI between the O_{2p} bands and the upper Hubbard bands as well as between e_g^π and e_g^σ bands. More interesting is the increase in spectral weight at low energies (up to 3 eV) upon cooling metallic V_2O_3 from $T=400$ K to $T=200$ K, in accord with previous reports.[41,42] However, in contrast to previous reports, our data extends up to much higher energies (6 eV) and show that this increase in spectral weight is only partially accounted for by a corresponding decrease between 3 eV and 6 eV. This is very different from what is expected in cooling a conventional metal that is well described by band theory. In a conventional metal, the Drude peak narrows as the scattering rate decreases with temperature but the spectral weight is conserved within the bandwidth. In V_2O_3, the total t_{2g} bandwidth according to band theory is $\approx$2.5 eV.[65] Therefore, the temperature-driven spectral weight changes in metallic V_2O_3 that span energies at least up to 6 eV cannot be simply explained within a single-particle picture.

In the PMM phase of V_2O_3, the energy $K(\omega)$ does not reach the intraband value of VO_2 (0.12 eV) until about 3 eV of the incident photon energy, well into the region of V-V interband transitions. If we assume that only the narrow Drude peak in PMM V_2O_3 represents the intraband part of the energy and spectral weight, then we obtain $K(\omega) \approx 0.012$ eV, the kinetic energy of delocalized carriers, which is nearly six percent of the band value in V_2O_3 (Ref. 42) and significantly less than in VO_2. This will place PMM V_2O_3 in the strongly correlated limit, with a higher degree of correlations compared to rutile VO_2. Therefore, correlation effects are more pronounced in the metallic phase (PMM) near a magnetically ordered Mott insulator (AFI V_2O_3) compared to the rutile metallic phase (R) near the Mott insulator (M_1 VO_2) that is charge ordered with quasi-one-dimensional chains of vanadium pairs. Nevertheless, we emphasize that charge dynamics of rutile metallic VO_2 cannot be described without taking into account correlation effects.[56]

In Fig. 5 we plot the temperature dependence of the low energy optical conductivity of the PMM. The difference between the $T=200$ K and $T=400$ K optical conductivity is plotted in the inset of Fig. 5. The temperature-induced change in the conductivity for the peak at 0.5 eV in the PMM is very similar to that of the Drude peak. This supports our assignments of the Drude peak to the coherent quasiparticles in a_{1g} and the peak at 0.5 eV to intersite transitions between the incoherent carriers in e_g^π and coherent empty states of a_{1g} character. This is because the coherent quasiparticles are expected to show a strong temperature dependence compared to the charge carriers in e_g^π that are well above their coherence temperature.[68]

V. SUMMARY AND OUTLOOK

We have investigated the optical constants of VO_2 and V_2O_3 films over a wide frequency and temperature range. We tracked changes of the optical conductivity $\sigma_1(\omega)$ and spectral weight $SW(\omega)$ across the metal-insulator transitions in both materials. In both VO_2 and V_2O_3, the changes in $\sigma_1(\omega)$ and $SW(\omega)$ extend up to and beyond 6 eV indicating the importance of electronic correlations to the metal-insulator transitions. From the kinetic energy of charge carriers, we deduce that rutile metallic VO_2 and paramagnetic metallic V_2O_3 are correlated metals, with metallic V_2O_3 showing a higher degree of correlations. Our optics data show that the energy gaps are nearly the same magnitude in M_1 insulating VO_2 and antiferromagnetic insulating V_2O_3, which is interesting given the different lattice structures, magnetic properties, and number of d electrons in the two oxides. While it may be a coincidence that the energy gaps have nearly the same magnitude, it is more likely that the Hubbard U is the common primary factor in determining the energy gap magnitude in both these oxides. Charge ordering of vanadium ions imparts a quasi-one-dimensional character to insulating VO_2 resulting in narrow a_{1g} bands and sharp optical transitions between these bands with possible excitonic effects.

When electron-phonon interactions cause metal-insulator transitions to occur, as, for example, in V_3O_5 and Fe_3O_4, the spectral weight across the phase transitions is conserved on the energy scale of 1 eV.[69,70] For the MIT in VO_2 and V_2O_3, the sum rule is not exhausted up to a much higher energy scale of 6 eV, which clearly highlights the important role of electron-electron correlations in the MIT in both these vanadium oxides. Temperature-induced changes in optical conductivity and spectral weight are seen over similar large energy scales in other transition metal oxides that are Mott insulators, for example, YVO_3, $LaVO_3$, and $LaMnO_3$.[46,71–73]

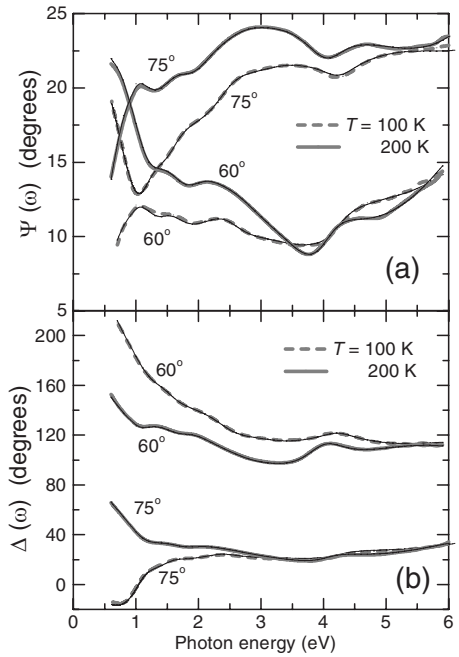

FIG. 6. The ellipsometric constants $\Psi(\omega)$ and $\Delta(\omega)$ for the V_2O_3 film/sapphire substrate system are plotted as a function of photon energy in panels (a) and (b), respectively. The thick dashed gray curves are the data for the AFI phase of V_2O_3 at $T=100$ K for two angles of incidence (60° and 75°). The thick solid gray curves are the corresponding data for the PMM phase of V_2O_3 at $T=200$ K. The thin solid black curves are fits to the data based on the model described in the section on experimental methods.

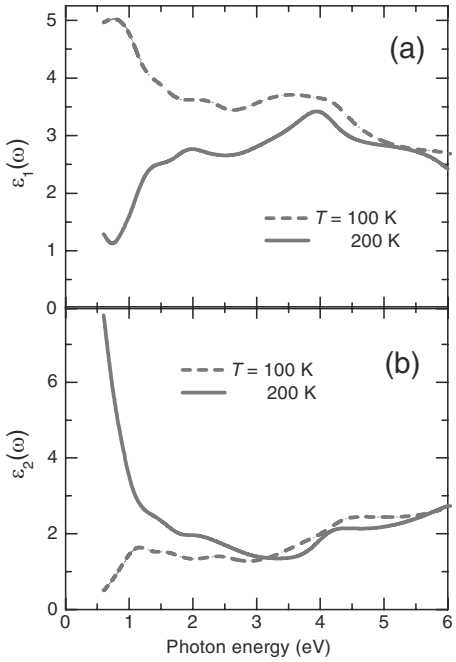

FIG. 7. The real part $\varepsilon_1(\omega)$ and imaginary part $\varepsilon_2(\omega)$ of the optical constants for the V_2O_3 film are plotted as a function of photon energy in panels (a) and (b), respectively. The optical constants of V_2O_3 film plotted in this figure are obtained from modeling of the ellipsometric constants of the film-substrate system displayed in Figs. 6(a) and 6(b). The dashed curves are optical constants of the AFI phase of V_2O_3 at $T=100$ K. The solid curves are the optical constants for the PMM phase of V_2O_3 at $T=200$ K.

Doped Mott insulators like the cuprates also exhibit shifts of spectral weight from similar high energies to lower energies upon chemical doping.[2,63,73] In this context, our work indicates that Mott physics plays the dominant role in the MIT in VO_2 and V_2O_3, whereas electron-phonon interactions and the lattice rearrangement play a competing role. Nevertheless, a complete picture of the MIT should take into account the electron-lattice interactions in addition to electron-electron interactions.[74]

Recent work on VO_2 provides evidence that the MIT is a Mott transition driven by Brinkman-Rice mass divergence of the quasiparticles.[22,23] The divergent effective mass occurs in metallic nanoscale puddles that first nucleate in the insulating host in the vicinity of the insulator-to-metal transition. The metallic nanopuddles were observed directly by scanning near-field infrared miscroscopy. These new data in combination with far-field infrared spectroscopy measurements demonstrated that the effective mass in the metallic nanopuddles of VO_2 is significantly enhanced compared to the macroscopic rutile metal at higher temperatures. There is evidence of heavy quasiparticles in metallic V_2O_3 in the literature although mass divergence in V_2O_3 has not been explicitly demonstrated.[39,75] Therefore, V_2O_3 needs to be studied using the experimental techniques and analytical procedures employed on VO_2 in Ref. 22 because it is also possible that in V_2O_3 mass divergence occurs in the vicinity of the MIT where there is a tendency toward phase separation.

In this work, we have displayed evidence of the importance of correlation effects to the metal-insulator transitions in VO_2 and V_2O_3. A corollary is that structural changes in both materials cannot explain the large energy gaps in the insulating phases and the large energy scales that are associated with the metal-insulator transitions. Nevertheless, structural changes cannot be easily explained within Mott physics and likely involve electron-phonon coupling, which should be taken into account in any realistic description of the metal-insulator transitions. Moreover, the metal-insulator transition temperatures in both the vanadium oxides we have investigated are an order of magnitude less than the energy gaps in the insulating phases, and there is hardly any satisfactory quantitative explanation for this. However, there are qualitative suggestions emphasizing the importance of the multiorbital character of these vanadium oxides.[67] Future optical and infrared work on single crystals and/or highly oriented, epitaxial films of VO_2 and V_2O_3 is required to determine changes in orbital occupation that accompany the metal-insulator transition. Nevertheless, the comprehensive nature of our experiments reported here sets the stage for more in-depth theoretical analysis and specifically computational analysis of the metal-insulator transitions since computational (DMFT and GW) results can be directly compared to optics data.

Note added in proof. A paper recently appeared by Baldassarre *et al.*[77] on infrared measurements on V_2O_3 crystals. In this paper, the Drude part of the conductivity of the V_2O_3

crystals in the metallic phase is higher than that of the V_2O_3 films studied in our work.

ACKNOWLEDGMENTS

We gratefully acknowledge discussions with S. Biermann, J. Tomczak, A. J. Millis, G. Kotliar, M. Fogler, J. E. Hirsch, T. Tiwald, and D. van der Marel. This work was supported by Department of Energy Grant No. DE-FG03-00ER45799 and by ETRI.

APPENDIX

For ellipsometry at cryogenic temperatures, the sample has to be kept in ultrahigh vacuum (UHV) to prevent formation of a layer of ice. The ellipsometric measurements (incident photon energies 0.6–6 eV) on the V_2O_3 film at low temperatures ($100\ \mathrm{K} \leqslant T \leqslant 300\ \mathrm{K}$) were performed in a vacuum of $\approx 10^{-9}$ torr in a custom-built UHV chamber. The incident and reflected light pass through UHV compatible optical windows. The change in the polarization state of light due to the windows was accounted for via calibration in vacuum using a standard silicon wafer with a 200-Å-thick layer of SiO_2.

The ellipsometric constants $\Psi(\omega)$ and $\Delta(\omega)$ of the V_2O_3 film on a sapphire substrate are plotted in Figs. 6(a) and 6(b) for the V_2O_3 film in the AFI phase ($T=100$ K) and in the PMM phase ($T=200$ K). The data presented were obtained for two angles of incidence (60° and 75°). Also plotted are fits to the data based on the model described in the section on experimental methods. The optical constants of the V_2O_3 film for the AFI and PMM phases are plotted in Figs. 7(a) and 7(b) and are obtained from modeling of the ellipsometric constants of the film-substrate system.

*mumtaz@physics.ucsd.edu

†Permanent address: Los Alamos National Laboratory, Mail Stop K771, Los Alamos, NM 87545, USA.

[1] N. F. Mott, *Metal-Insulator Transitions* (Taylor & Francis, London, 1990).

[2] M. Imada, A. Fujimori, and Y. Tokura, Rev. Mod. Phys. **70**, 1039 (1998).

[3] J. B. Goodenough, J. Solid State Chem. **3**, 490 (1971).

[4] A. Zylbersztejn and N. F. Mott, Phys. Rev. B **11**, 4383 (1975).

[5] R. M. Wentzcovitch, W. W. Schulz, and P. B. Allen, Phys. Rev. Lett. **72**, 3389 (1994); **73**, 3043 (1994).

[6] V. Eyert, Ann. Phys. **11**, 650 (2002).

[7] S. Biermann, A. Poteryaev, A. I. Lichtenstein, and A. Georges, Phys. Rev. Lett. **94**, 026404 (2005).

[8] M. W. Haverkort, Z. Hu, A. Tanaka, W. Reichelt, S. V. Streltsov, M. A. Korotin, V. I. Anisimov, H. H. Hsieh, H.-J. Lin, C. T. Chen, D. I. Khomskii, and L. H. Tjeng, Phys. Rev. Lett. **95**, 196404 (2005).

[9] T. C. Koethe, Z. Hu, M. W. Haverkort, C. Schüßler-Langeheine, F. Venturini, N. B. Brookes, O. Tjernberg, W. Reichelt, H. H. Hsieh, H.-J. Lin, C. T. Chen, and L. H. Tjeng, Phys. Rev. Lett. **97**, 116402 (2006).

[10] H. Abe, M. Terauchi, M. Tanaka, S. Shin, and Y. Ueda, Jpn. J. Appl. Phys., Part 1 **36**, 165 (1997).

[11] J. P. Pouget, H. Launois, T. M. Rice, P. Dernier, A. Gossard, G. Villeneuve, and P. Hagenmuller, Phys. Rev. B **10**, 1801 (1974).

[12] J. P. Pouget, H. Launois, J. P. D'Haenens, P. Merenda, and T. M. Rice, Phys. Rev. Lett. **35**, 873 (1975).

[13] M. Gupta, A. J. Freeman, and D. E. Ellis, Phys. Rev. B **16**, 3338 (1977).

[14] D. Paquet and P. Leroux-Hugon, Phys. Rev. B **22**, 5284 (1980).

[15] T. M. Rice, H. Launois, and J. P. Pouget, Phys. Rev. Lett. **73**, 3042 (1994).

[16] A. Continenza, S. Massidda, and M. Posternak, Phys. Rev. B **60**, 15699 (1999).

[17] H. T. Kim, B. G. Chae, D. H. Youn, S. L. Maeng, G. Kim, K. Y. Kang, and Y. S. Lim, New J. Phys. **6**, 52 (2004).

[18] M. S. Laad, L. Craco, and E. Müller-Hartmann, Europhys. Lett. **69**, 984 (2005).

[19] H. T. Kim, Y. W. Lee, B. J. Kim, B. G. Chae, S. J. Yun, K. Y. Kang, K. J. Han, K. J. Yee, and Y. S. Lim, Phys. Rev. Lett. **97**, 266401 (2006).

[20] E. Arcangeletti, L. Baldassarre, D. Di Castro, S. Lupi, L. Malavasi, C. Marini, A. Perucchi, and P. Postorino, Phys. Rev. Lett. **98**, 196406 (2007).

[21] D. J. Hilton, R. P. Prasankumar, S. Fourmaux, A. Cavalleri, D. Brassard, M. A. El Khakani, J. C. Kieffer, A. J. Taylor, and R. D. Averitt, Phys. Rev. Lett. **99**, 226401 (2007).

[22] M. M. Qazilbash, M. Brehm, Byung-Gyu Chae, P.-C. Ho, G. O. Andreev, Bong-Jun Kim, Sun Jin Yun, A. V. Balatsky, M. B. Maple, F. Keilmann, Hyun-Tak Kim, and D. N. Basov, Science **318**, 1750 (2007).

[23] W. F. Brinkman and T. M. Rice, Phys. Rev. B **2**, 4302 (1970).

[24] H. T. Kim, Physica C **341-348**, 259 (2000).

[25] P. D. Dernier and M. Marizio, Phys. Rev. B **2**, 3771 (1970).

[26] C. Castellani, C. R. Natoli, and J. Ranninger, Phys. Rev. B **18**, 4945 (1978); **18**, 4967 (1978); **18**, 5001 (1978).

[27] S. Y. Ezhov, V. I. Anisimov, D. I. Khomskii, and G. A. Sawatzky, Phys. Rev. Lett. **83**, 4136 (1999).

[28] F. Mila, R. Shiina, F.-C. Zhang, A. Joshi, M. Ma, V. Anisimov, and T. M. Rice, Phys. Rev. Lett. **85**, 1714 (2000).

[29] A. Joshi, Michael Ma, and F. C. Zhang, Phys. Rev. Lett. **86**, 5743 (2001).

[30] S. Di Matteo, N. B. Perkins, and C. R. Natoli, Phys. Rev. B **65**, 054413 (2002).

[31] A. Tanaka, J. Phys. Soc. Jpn. **71**, 1091 (2002).

[32] W. Bao, C. Broholm, G. Aeppli, P. Dai, J. M. Honig, and P. Metcalf, Phys. Rev. Lett. **78**, 507 (1997).

[33] L. Paolasini, C. Vettier, F. de Bergevin, F. Yakhou, D. Mannix, A. Stunault, W. Neubeck, M. Altarelli, M. Fabrizio, P. A. Metcalf, and J. M. Honig, Phys. Rev. Lett. **82**, 4719 (1999).

[34] J.-H. Park, L. H. Tjeng, A. Tanaka, J. W. Allen, C. T. Chen, P. Metcalf, J. M. Honig, F. M. F. de Groot, and G. A. Sawatzky, Phys. Rev. B **61**, 11506 (2000).

[35] S.-K. Mo, J. D. Denlinger, H.-D. Kim, J.-H. Park, J. W. Allen, A. Sekiyama, A. Yamasaki, K. Kadono, S. Suga, Y. Saitoh, T.

Muro, P. Metcalf, G. Keller, K. Held, V. Eyert, V. I. Anisimov, and D. Vollhardt, Phys. Rev. Lett. **90**, 186403 (2003).
[36] A. S. Barker, Jr., H. W. Verleur, and H. J. Guggenheim, Phys. Rev. Lett. **17**, 1286 (1966).
[37] H. W. Verleur, A. S. Barker, Jr., and C. N. Berglund, Phys. Rev. **172**, 788 (1968).
[38] S. Shin, S. Suga, M. Taniguchi, M. Fujisawa, H. Kanzaki, A. Fujimori, H. Daimon, Y. Ueda, K. Kosuge, and S. Kachi, Phys. Rev. B **41**, 4993 (1990).
[39] G. A. Thomas, D. H. Rapkine, S. A. Carter, T. F. Rosenbaum, P. Metcalf, and D. F. Honig, J. Low Temp. Phys. **95**, 33 (1994).
[40] G. A. Thomas, D. H. Rapkine, S. A. Carter, A. J. Millis, T. F. Rosenbaum, P. Metcalf, and J. M. Honig, Phys. Rev. Lett. **73**, 1529 (1994).
[41] M. J. Rozenberg, G. Kotliar, H. Kajueter, G. A. Thomas, D. H. Rapkine, J. M. Honig, and P. Metcalf, Phys. Rev. Lett. **75**, 105 (1995).
[42] M. J. Rozenberg, G. Kotliar, and H. Kajueter, Phys. Rev. B **54**, 8452 (1996).
[43] H. S. Choi, J. S. Ahn, J. H. Jung, T. W. Noh, and D. H. Kim, Phys. Rev. B **54**, 4621 (1996).
[44] K. Okazaki, S. Sugai, Y. Muraoka, and Z. Hiroi, Phys. Rev. B **73**, 165116 (2006).
[45] J. M. Tomczak, F. Aryasetiawan, and S. Biermann, arXiv:0704.0902 (unpublished); J. M. Tomczak, Ph.D. thesis, Ecole Polytechnique, 2007.
[46] A. A. Tsvetkov, F. P. Mena, P. H. M. van Loosdrecht, D. van der Marel, Y. Ren, A. A. Nugroho, A. A. Menovsky, I. S. Elfimov, and G. A. Sawatzky, Phys. Rev. B **69**, 075110 (2004).
[47] *Handbook of Ellipsometry*, edited by H. G. Tompkins and E. A. Irene (William Andrew Publishing, Springer Verlag, Heidelberg, 2005).
[48] In contrast to VO_2 films grown on SiO_2/Si substrates and studied by x-ray absorption spectroscopy in Ref. 76, our VO_2 and V_2O_3 films grown on lattice matched sapphire substrates do not show signs of deterioration after cycling several times through the MIT. This was verified by ellipsometric and reflectance measurements that give reproducible data in the insulating and metallic phases before and after cycling through the MIT.
[49] B. G. Chae, H. T. Kim, S. J. Yun, B. J. Kim, Y. W. Lee, D. H. Youn, and K. Y. Kang, Electrochem. Solid-State Lett. **9**, C12 (2006).
[50] S. J. Yun, B.-G. Chae, J. W. Lim, J. S. Noh, and H. T. Kim, Electrochem. Solid-State Lett. (to be published).
[51] P. A. Metcalf, S. Guha, L. P. Gonzalez, J. O. Barnes, E. B. Slamovich, and J. M. Honig, Thin Solid Films **515**, 3421 (2007).
[52] K. S. Burch, J. Stephens, R. K. Kawakami, D. D. Awschalom, and D. N. Basov, Phys. Rev. B **70**, 205208 (2004).
[53] M. Schubert, T. E. Tiwald, and C. M. Herzinger, Phys. Rev. B **61**, 8187 (2000).
[54] We have studied thin films of VO_2 and V_2O_3 in which the phonon features are fairly weak and are partially obscured by much stronger phonon features from the sapphire substrate. Infrared studies of single crystals of VO_2 and V_2O_3 are required to precisely quantify the phonon contributions to the optical conductivity and the changes that occur in the phonons across the MIT.
[55] K. Okazaki, H. Wadati, A. Fujimori, M. Onoda, Y. Muraoka, and Z. Hiroi, Phys. Rev. B **69**, 165104 (2004).
[56] M. M. Qazilbash, K. S. Burch, D. Whisler, D. Shrekenhamer, B. G. Chae, H. T. Kim, and D. N. Basov, Phys. Rev. B **74**, 205118 (2006).
[57] G. E. Jellison, Jr. and F. A. Modine, Appl. Phys. Lett. **69**, 371 (1996); **69**, 2137 (1996).
[58] N. Tsuda, K. Nasu, A. Fujimori, and K. Siratori, *Electronic Conduction in Oxides* (Springer-Verlag, Berlin, 2000).
[59] R. Schuster, M. Knupfer, and H. Berger, Phys. Rev. Lett. **98**, 037402 (2007).
[60] A. J. Millis, A. Zimmers, R. P. S. M. Lobo, N. Bontemps, and C. C. Homes, Phys. Rev. B **72**, 224517 (2005).
[61] J. S. Lee, M. W. Kim, and T. W. Noh, New J. Phys. **7**, 147 (2005).
[62] A. J. Millis, in *Strong Interactions in Low Dimensions*, edited by D. Baeriswyl and L. DeGiorgi (Springer Verlag, Berlin, 2004).
[63] D. N. Basov and T. Timusk, Rev. Mod. Phys. **77**, 721 (2005).
[64] C. Marianetti and G. Kotliar (unpublished).
[65] L. F. Mattheis, J. Phys.: Condens. Matter **6**, 6477 (1994).
[66] J. W. Taylor, T. J. Smith, K. H. Andersen, H. Capellmann, R. K. Kremer, A. Simon, O. Schärpf, K.-U. Neumann, and K. R. A. Ziebeck, Eur. Phys. J. B **12**, 199 (1999).
[67] D. I. Khomskii, Phys. Scr. **78**, CC2 (2005).
[68] A. I. Poteryaev, J. M. Tomczak, S. Biermann, A. Georges, A. I. Lichtenstein, A. N. Rubtsov, T. Saha-Dasgupta, and O. K. Andersen, Phys. Rev. B **76**, 085127 (2007).
[69] L. Baldassarre, A. Perucchi, E. Arcangeletti, D. Nicoletti, D. Di Castro, P. Postorino, V. A. Sidorov, and S. Lupi, Phys. Rev. B **75**, 245108 (2007).
[70] L. V. Gasparov, D. B. Tanner, D. B. Romero, H. Berger, G. Margaritondo, and L. Forrò, Phys. Rev. B **62**, 7939 (2000).
[71] S. Miyasaka, Y. Okimoto, and Y. Tokura, J. Phys. Soc. Jpn. **71**, 2086 (2002).
[72] N. N. Kovaleva, A. V. Boris, C. Bernhard, A. Kulakov, A. Pimenov, A. M. Balbashov, G. Khaliullin, and B. Keimer, Phys. Rev. Lett. **93**, 147204 (2004).
[73] S. V. Dordevic and D. N. Basov, Ann. Phys. **15**, 545 (2006).
[74] P. Pfalzer, G. Obermeier, M. Klemm, S. Horn, and M. L. denBoer, Phys. Rev. B **73**, 144106 (2006).
[75] D. B. McWhan, J. P. Remeika, S. D. Bader, B. B. Triplett, and N. E. Phillips, Phys. Rev. B **7**, 3079 (1973).
[76] D. Ruzmetov, S. D. Senanayake, and S. Ramanathan, Phys. Rev. B **75**, 195102 (2007).
[77] L. Baldassarre *et al.*, arXiv:0710.1247, Phys. Rev. B (to be published).